In-Situ Construction of MoO_2/In_2O_3 Heterostructures to Accelerate Reaction Kinetics for Electrocatalytic Nitrogen Reduction

Yuhang Cheng,[a] Jianlong Chen,[a] Hangning Liu,[a] Qi Wang,[a] Manting Tang,[a] Xuyun Guo,[b] Valeria Nicolosi,[b] Linghao Su,[a,*] Jie Wang[a,*]

[a] Qingdao Engineering Research Center of Agricultural Recycling Economy Materials, College of Chemistry and Pharmaceutical Sciences, Qingdao Agricultural University, Qingdao 266109, P. R. China

[b] School of Chemistry, Centre for Research on Adaptive Nanostructures and Nanodevices (CRANN) and Advanced Materials Bio-Engineering Research Centre (AMBER), Trinity College Dublin, Dublin D02PN40, Ireland

Experimental Section

Material synthesis

In a 50 mL beaker, 10 mmol of indium chloride ($InCl_3$), 2 mmol of ammonium molybdate ($(NH_4)_6Mo_7O_{24}\cdot 4H_2O$), 25 mmol of urea, and 10 mmol of ammonium fluoride (NH_4F) were sequentially added. Subsequently, 35 mL of deionized water was introduced using a graduated cylinder, and the mixture was stirred magnetically at room temperature for 30 min to ensure complete dissolution and homogeneous dispersion of all components. A piece of commercial copper foam (CF) was cut to dimensions of 3 cm × 4 cm and cleaned by immersion in 0.1 mol L^{-1} hydrochloric acid solution for 10 minutes to remove surface oxides and impurities. The etched CF was then thoroughly rinsed with deionized water until neutral pH was achieved, ensuring complete removal of residual acid. The cleaned CF substrate and the as-prepared precursor solution were subsequently transferred into a 50 mL Teflon-lined stainless-steel autoclave. The sealed autoclave was heated at 110 °C for 10 hours in an oven to carry out the hydrothermal reaction.

Following hydrothermal synthesis, the sample was retrieved and sequentially washed three times with deionized water and ethanol to remove residual reactants and byproducts. The cleaned product was then placed in a porcelain boat and loaded into a tube furnace. Prior to thermal treatment, the furnace chamber was purged with argon (Ar) for 30 minutes to establish an inert atmosphere. Under a continuous Ar flow, the sample was heated to 350 °C at a ramp rate of 5 °C per minute and held at this temperature for 2 hours to complete calcination. Afterward, the furnace was allowed to cool naturally to room temperature, yielding the final MoO_2/In_2O_3/CF electrocatalyst. For comparative purposes, pristine In_2O_3/CF was synthesized using an identical procedure, omitting the molybdenum precursor.

Physical Characterizations

The microstructural morphology of the catalysts was meticulously characterized using a JEOL JSM-IT500 scanning electron microscopy (SEM). Detailed insights into their nanoscale structure were further obtained through transmission electron microscopy (TEM) and annular dark field scanning TEM (ADF-STEM), which were performed using an uncorrected FEI Titan with Schottky field emission S-FEG source operated at 300 kV. The microscope was equipped with Gatan Quantum electron energy-loss spectroscopy (EELS) detectors for elemental analysis. The EELS spectrometer was operated with an energy dispersion of 0.5 eV per channel. The crystalline phases of the catalysts were analyzed via Powder X-ray Diffraction (XRD) over a 2θ range of 10 - 80°, using a Bruker D8 ADVANCE diffractometer equipped with Cu Kα radiation (λ = 0.15418 nm). Surface chemical states and electronic structures were probed by X-ray Photoelectron Spectroscopy (XPS), conducted on a PHI-5000 VersaProbe III spectrometer (Thermo Scientific, USA) with an Al Kα X-ray source, and calibrated using the C 1s peak at 284.8 eV as a reference. UV-Vis absorption

measurements were performed on a UV–Vis spectrophotometer (Shimadzu, UV-2600).

Determination of NH_3

The indophenol blue colorimetric method was employed to determine the ammonia concentration in the electrolyte. First, a series of standard NH_4Cl solutions with varying concentrations in 0.10 M Na_2SO_4 were prepared to establish the calibration curve. Subsequently, 50 μL of sodium nitroferricyanide dihydrate (1 wt%), 250 μL of a solution containing 2 M NaOH, sodium citrate, and salicylic acid (5 wt%), and 50 μL of NaClO (0.05 M) in 2 M NaOH were added to a 5 mL aliquot of the sample solution (0.10 M Na_2SO_4). After standing for 1 h, the absorbance of the mixed solutions was measured at a wavelength of 695 nm. The calibration curve exhibited a good linear relationship, which was then used to calculate the ammonia concentration after the electrochemical tests.

Electrochemical measurements

The electrochemical performance was assessed using a CHI 660F electrochemical workstation (CH Instruments) with a standard three-electrode setup. The working electrode was cut into a 1 cm × 1 cm size and clamped by an electrode holder. A platinum electrode and an Ag/AgCl electrode were used as the counter electrode and reference electrode, respectively. All electrochemical measurements were conducted in 0.1 M Na_2SO_4 electrolyte.

All potentials measured against the Ag/AgCl reference electrode were converted to the reversible hydrogen electrode (RHE) scale using the following equation:

$$E_{\mathrm{RHE}} = E_{\mathrm{Ag/AgCl}} + 0.197 + 0.059 \times \mathrm{pH} \qquad (1)$$

Linear sweep voltammetry (LSV) was performed at a scan rate of 5 mV s^{-1} with a potential range of 0.30 V to -1.0 V vs. RHE. Chronoamperometry (i-t) tests were conducted at various potentials for 1 hour to quantify NH_3 production. The NH_3 yield rates and Faradaic efficiencies (FE) were quantified using the indophenol blue method with UV-Vis spectrophotometry. The electrochemical active surface area (ECSA) was assessed by measuring the double-layer capacitance (C_{dl}) via cyclic voltammetry (CV) in the non-Faradaic region. CV measurements were performed in the potential range from -0.21 V to -0.11 V (vs. RHE) at various scan rates (20, 40, 60, 80, and 100 mV s^{-1}). The current density differences ($\Delta j = j_a - j_c$) at a fixed potential were plotted against the scan rates, and the slope corresponds to twice the C_{dl} value. Distribution of relaxation times (DRT) analysis was performed to gain deeper insights into the electrochemical processes. Electrochemical impedance spectroscopy (EIS) was conducted in the frequency range from 0.01 Hz to 100 kHz with an AC amplitude of 5 mV and a quiet time of 2 seconds. The DRT plots were derived from the EIS data to analyze the charge transfer kinetics.

The stability of MoO_2/In_2O_3/CF was evaluated by consecutive chronoamperometry tests over 8 cycles at -0.60 V vs. RHE, with each cycle lasting 1 hour. The NH_3 yield rates and FE were

measured after each cycle.

The NH_3 yield rate was calculated using the following equation:

$$NH_3\ yield\ rate = \frac{C_{NH_3} \times V}{S \times t}\ \mu g\ h^{-1}\ cm^{-2} \quad (2)$$

C_{NH_3} = measured NH_3 concentration (μg mL^{-1})

V = volume of electrolyte in the cathode chamber (mL)

S = geometric area of the working electrode (cm^2)

t = electrolysis time (hour)

The FE for NH_3 production was calculated using the following equation:

$$FE_{NH_3}(\%) = \frac{n \times F \times C_{NH_3} \times V}{M_{NH_3} \times Q} \times 100\% \quad (3)$$

n = number of electrons transferred for N_2 to NH_3 (n = 3 for N atom, or n = 6 for N_2 molecule; here we use n = 3 for NH_3 quantification)

F = Faraday constant (96485 C mol^{-1})

C_{NH_3} = measured NH_3 concentration (mol L^{-1})

V = volume of electrolyte (L)

M_{NH_3} = molar mass of NH_3 (17.03 g mol^{-1})

Q = total charge passed during electrolysis (C)

To evaluate the intrinsic activity of each active site, the current density was normalized by the double-layer capacitance:

$$j_K^{norm} = \frac{j}{C_{dl}} \quad (4)$$

j_K^{norm} = normalized current density (mA mF^{-1})

j = current density at a given potential (mA cm^{-2})

C_{dl} = double-layer capacitance (mF cm^{-2})

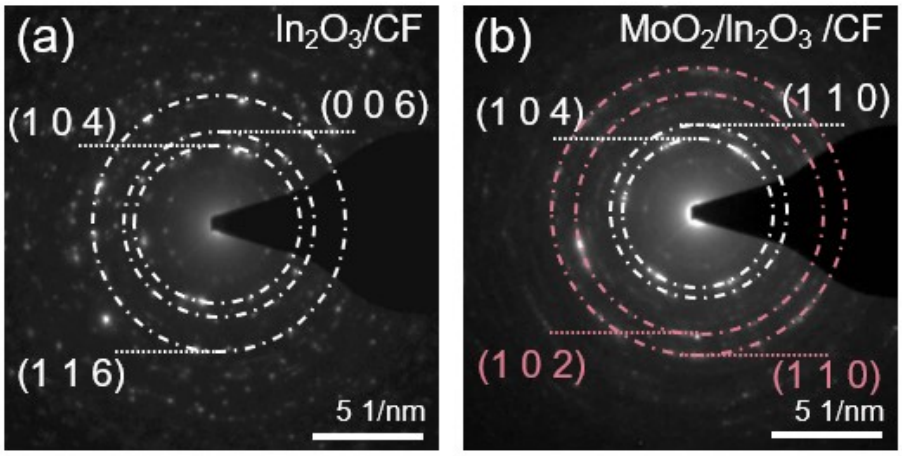

Fig. S1 SAED pattern of In_2O_3/CF and $MoO_2/In_2O_{3/CF}$. The white line corresponds to the In_2O_3/CF phase, while the pink line corresponds to the MoO_2 phase.

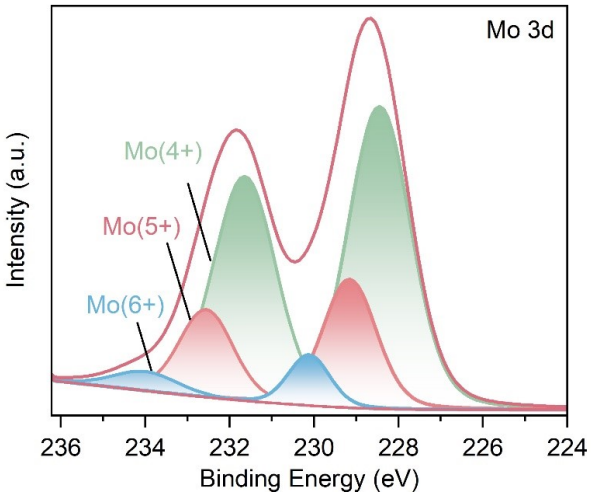

Fig. S2 High-resolution Mo 3d XPS spectrum.

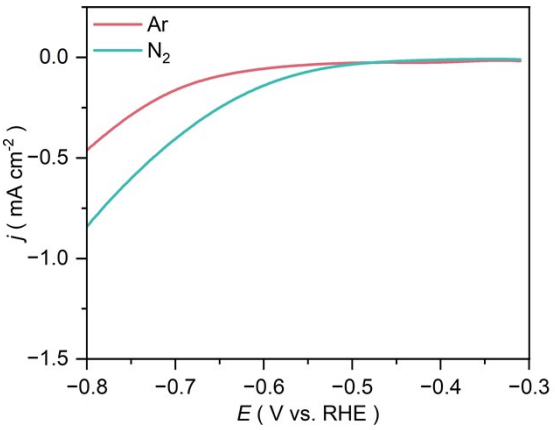

Fig. S3 LSV curves of pristine In_2O_3/CF in Ar- and N_2- saturated electrolyte.

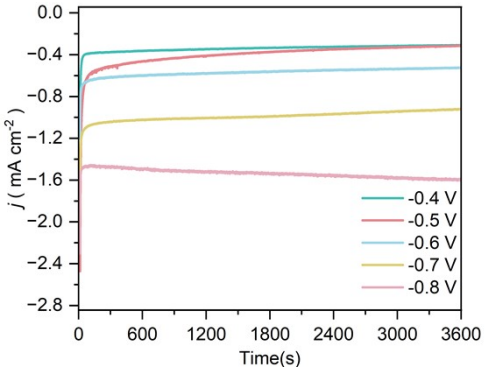

Fig. S4 Chronoamperometry curves of pristine In_2O_3/CF at different potentials in N_2- saturated electrolyte.

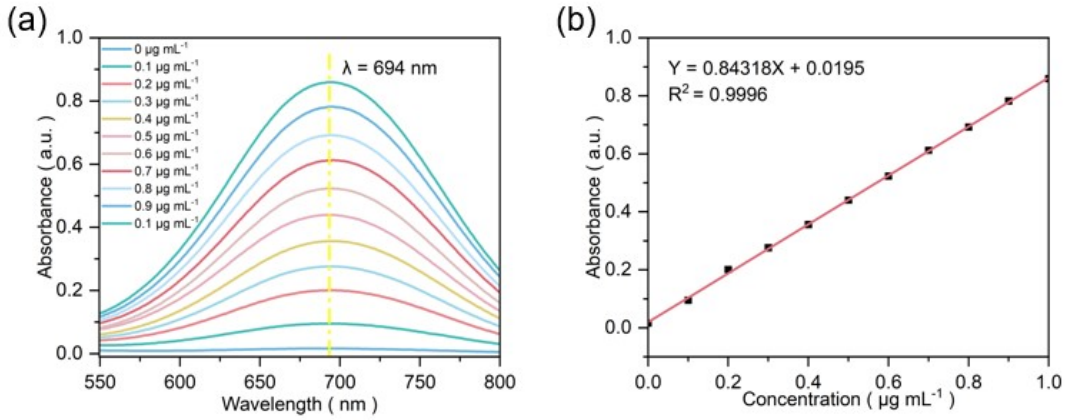

Fig. S5 (a) UV-Vis absorption spectra of NH_3 determination via an indophenol blue method; (b) corresponding calibration curve.

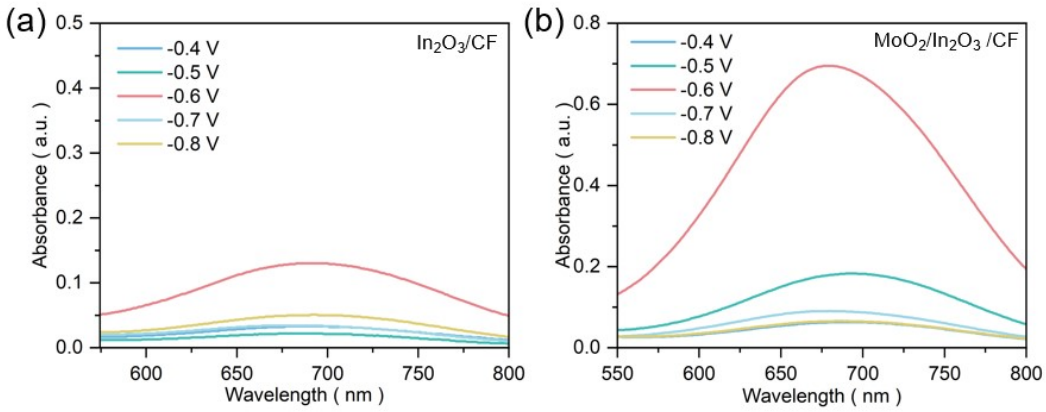

Fig. S6 UV-Vis absorption spectra of the electrolyte obtained using (a) In_2O_3/CF and (b) MoO_2/In_2O_3/CF as catalysts at different potentials.

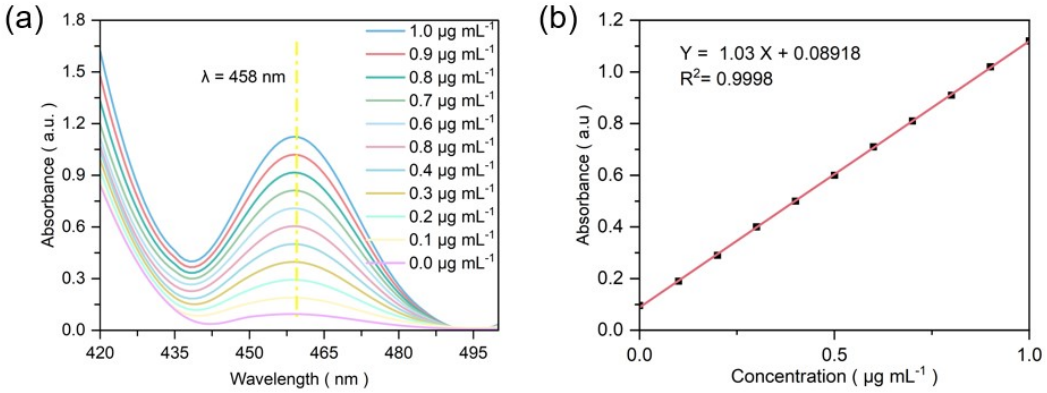

Fig. S7 UV-Vis absorption spectra of N_2H_4 determination via indophenol blue method, (b) corresponding calibration curve.

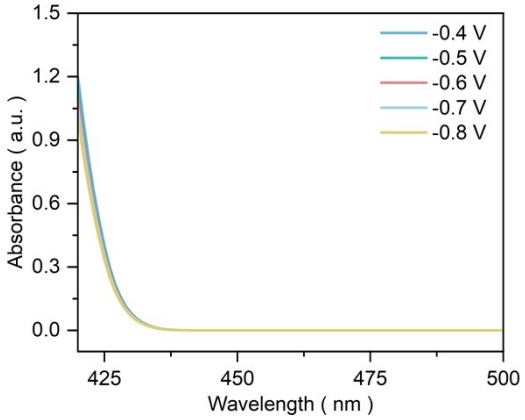

Fig. S8 UV-Vis absorption spectra of the electrolyte obtained using MoO_2/In_2O_3/CF as catalysts at different potentials.

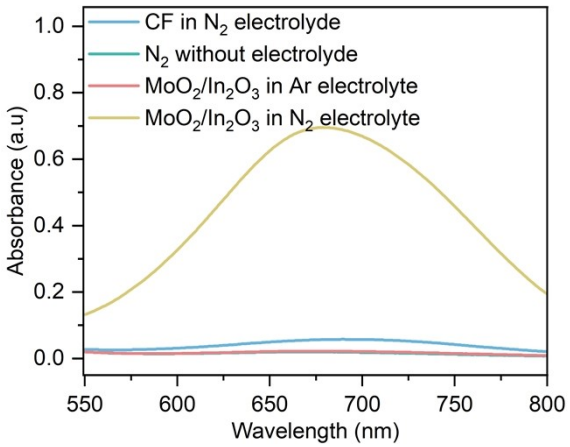

Fig. S9 UV-Vis absorption spectra after using CF as the work electrode in N_2-saturated electrolyte, N_2 fed directly into the electrolyte without electric charge, and MoO_2/In_2O_3/CF as the working electrode in Ar- and N_2-saturated electrolyte at -0.60 V (vs. RHE).

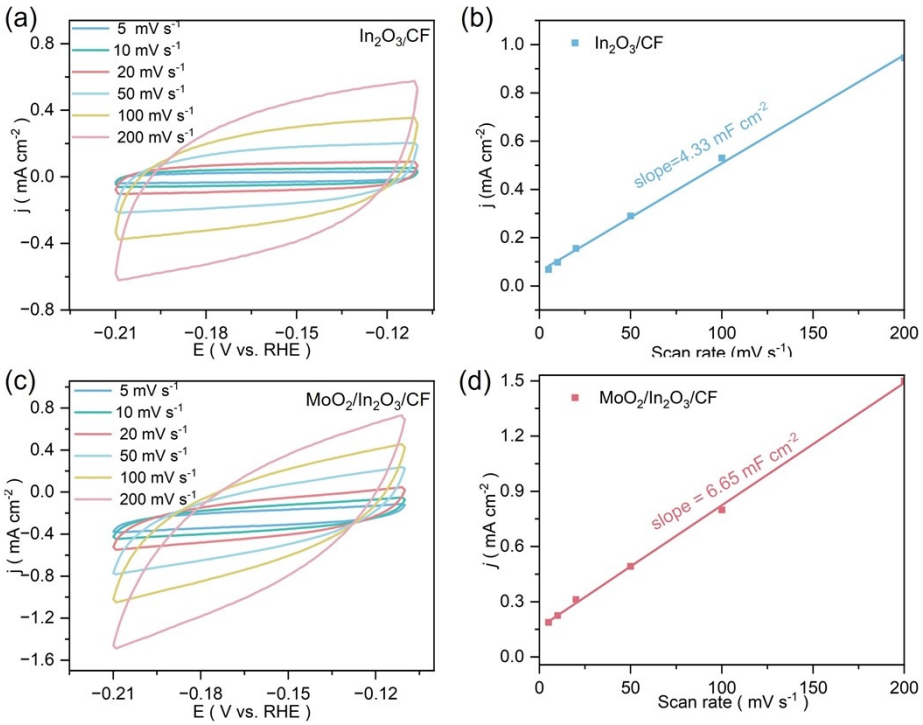

Fig. S10 (a) CV curves of pristine In_2O_3/CF at different scan rates; (b) corresponding charging current density differences vs. scan rates for C_{dl} calculation; (c) CV curves of MoO_2/In_2O_3/CF at different scan rates, (d) corresponding charging current density differences vs. scan rates for C_{dl} calculation.

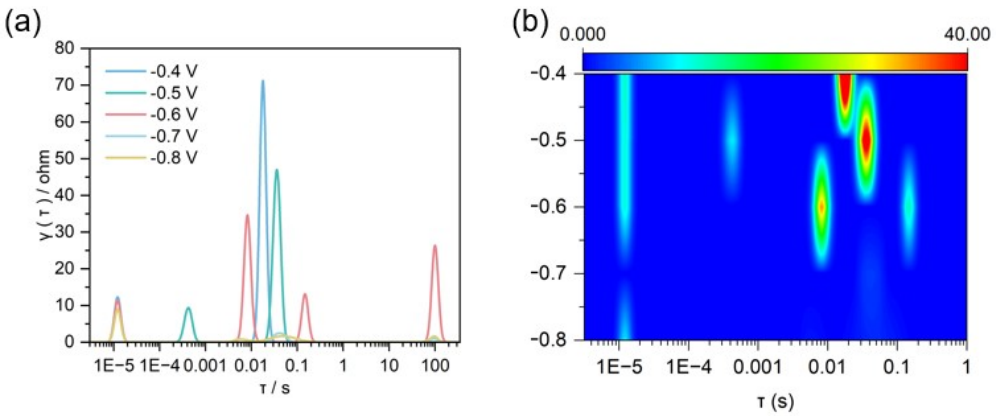

Fig. S11 (a) The relaxation time distribution vs. resistance diagram of In_2O_3/CF and (b) corresponding *in situ* relaxation time distribution vs. potential diagram.

Table S1. Comparison of NRR performance with typical oxide-based catalysts under similar electrochemical conditions.

Samples	Electrolyte	NH_3 yield rate	FE	Ref.
MoO_2/In_2O_3/CF	0.1 M Na_2SO_4	23.42 μg h^{-1} cm^{-2}	35.59%	This work
In_2O_3/CF	0.1 M Na_2SO_4	4.01 μg h^{-1} cm^{-2}	0.53%	This work
MoAlB SCs/CF	0.1 M KOH	9.2 μg h^{-1} cm^{-2}	30.1%	[1]
V-MnO_2/CF	0.005 M H_2SO_4	14.5 μg h^{-1} cm^{-2}	17.3%	[2]
Mo-Fe_2O_2/CF	0.1 M Na_2SO_4	21.3 μg h^{-1} cm^{-2}	11.2%	[3]
Ru-Cu /CF	0.1 M KOH	12.4 μg h^{-1} cm^{-2}	15.9%	[4]
Cu/Co-OH/CF	0.1 M KOH + 0.1 M KNO_3	16.7 μg h^{-1} cm^{-2}	22.1%	[5]
Fe-doped TiO_2	0.5 M $LiClO_4$	22.5 μg h^{-1} cm^{-2}	12.6%	[6]
Cr_2O_3	0.1 M Na_2SO_4	2.7 μg h^{-1} cm^{-2}	5.31%	[7]
MoO_3	0.1 M HCl	1.8 μg h^{-1} cm^{-2}	0.1%	[8]
$NiCo_2O_4$	0.1 M Na_2SO_4	17.8 μg h^{-1} cm^{-2}	5.3%	[9]
Sm_2O_3	0.1 M Li_2SO_4	15.3 μg h^{-1} cm^{-2}	21.7%	[10]
$MnMoO_4$	0.1 M Na_2SO_4	21.5 μg h^{-1} cm^{-2}	29.6%	[11]
MIL-Fe@Nb_2C	0.1 M HCl	8.9 μg h^{-1} cm^{-2}	20.8%	[12]
P-activated Cu	0.1 M KOH	7.7 μg h^{-1} cm^{-2}	13.2%	[13]

References

[1] Y. Fu, P. Richardson, K. Li, H. Yu, B. Yu, S. Donne, E. Kisi, T. Ma. *Nano-Micro Lett.* 2020, **12**, 65.

[2] L. Huang, X. Jiang, R. Deng, Q. Wang, T. Long, Y. Liang, Y. Li, Q. Jiang. *ACS Omega* 2025, **10**, 52944-52953.

[3] Z. Niu, L. Jiao, T. Zhang, X. Zhao, X. Wang, Z. Tan, L. Liu, S. Chen, X. Song. *ACS Appl. Mater. Interfaces* 2022, **14**, 55559-55567.

[4] K. Li, L. Ding, Z. Xie, G. Yang, S. Yu, W. Wang, D.A. Cullen, H.M. Meyer III, G. Hu, P. Ganesh, T.R. Watkins, F. Zhang. *ACS Appl. Mater. Interfaces* 2023, **15**, 11703-11712.

[5] L. Li, Q. Wang, Y. Chen, X. Chen, Q. Shi. *Front. Chem.* 2025, **13**, 1599613.

[6] T. Wu, X. Zhu, Z. Xing, S. Mou, C. Li, Y. Qiao, Q. Liu, Y. Luo, X. Shi, Y. Zhang, X. Sun. *Angew. Chem. Int. Ed.* 2019, **58**, 18449.

[7] L. Shi, Y. Yin, H. Wu, R. A. K. Hirani, X. Xu, J. Zhang, N. Rafique, A. H. Asif, S. Zhang, H. Sun. *Chin. J. Chem. Eng.* 2022, **41**, 358-365.

[8] D. Bao, Q. Zhang, F.L. Meng, H.X. Zhong, M.M. Shi, Y. Zhang, J.M. Yan, Q. Jiang, X.B. Zhang. *Adv. Mater.* 2017, **29**, 1604799.

[9] F. Lai, J. Feng, X. Ye, W. Zong, G. He, C. Yang, W. Wang, Y.-E. Miao, B. Pan, W. Yan, T. Liu, I.P.

Parkin. *J. Mater. Chem. A* 2020, **8**, 1652-1659.
[10] Y. Cheng, H. Nan, Q. Li, Y. Luo, K. Chu. *ACS Sustainable Chem. Eng.* 2020, **8**, 13908-13914.
[11] H. Yin, X. Xing, W. Zhang, J. Li, W. Xiong, H. Li. *Dalton Trans.* 2023, **52**, 16670-16679.
[12] H. Zhu, S. Xue, F. Zhao, Q. Hua, Z. Liang, X. Ren, L. Gao, T. Ma, A. Liu. *New J. Chem.* 2023, **47**, 15302-15308.
[13] J. Kim, C.H. Lee, Y.H. Moon, M.H. Lee, E.H. Kim, S.H. Choi, Y.J. Jang, J.S. Lee. *J. Energy Chem.* 2023, **84**, 394-401.